



Particle Measurement Sensor for *in situ* determination of phase structure of fluidized bed

Qiang Zhang, Cang Huang, Dong Jiang, Xiaobo Wei, Zhen Qian, Fei Wei*

Beijing Key Laboratory of Green Chemical Reaction Engineering and Technology, Department of Chemical Engineering, Tsinghua University, Beijing 100084, China

ARTICLE INFO

Article history:

Received 10 November 2008

Accepted 17 January 2009

Keywords:

Particle Measurement Sensor

Fluidized bed

Acceleration

Gas–solid two-phase flow

Phase structure

ABSTRACT

Based on three-dimensional (3D) acceleration sensing, an intelligent particle spy capable of detecting, transferring, and storing data, is proposed under the name of Particle Measurement Sensor (PMS). A prototype 60-mm-dia PMS was tested to track its freefall in terms of velocity and displacement, and served as a particle spy in a fluidized bed delivering the *in situ* acceleration information it detects. With increasing superficial gas velocity in the fluidized bed, the acceleration felt by PMS was observed to increase. The variance of the signals, which reflect the fluctuation, increased at first, reaching a maximum at the gas velocity (U_c) which marks the transition from bubbling to turbulent fluidization. Through probability density distribution (PDD) analysis, the PDD peak can be divided into the emulsion phase peak and the bubble phase peak. The average acceleration of emulsion and bubble phase increased, while the variance of both phases reached a maximum at U_c , at the same time. However, the difference between the variances of two phases reached the maximum at U_c . Findings of this study indicate that PMS can record independent *in situ* information. Further, it can provide other *in situ* measurements when equipped with additional multi-functional sensors.

© 2009 Chinese Society of Particuology and Institute of Process Engineering, Chinese Academy of Sciences. Published by Elsevier B.V. All rights reserved.

1. Introduction

Development of fluidization technique has spanned several decades, attesting to the importance of this technique in chemical engineering, thermal engineering, and metallurgy (Bi & Grace, 1995; Cheng, Wu, Zhu, Wei, & Jin, 2008; Kwauk, Li, & Liu, 2000; Wei et al., 2008; Zhu, Yu, Jin, Grace, & Issangya, 1995). One of the basic problems identified is tracing a particle's movement. In a fluidized bed, particles are clustered into different phases, the structures of which have been extensively studied in the last few decades. The interactions between particles and fields, or particles per se, have emerged as key issues. Nowadays, field information – such as field concentration, temperature, and velocity distribution – can be obtained by means of sensors: temperature by a thermocouple and solids holdup by a capacitance or an electrical conductivity probe. However, such sensors affect particle flow and the transport phenomena in the fields. Absolute pristine information is therefore not easily obtained, especially when the force between particles and fluid needs to be examined. Moreover, particle movement information is obtained indirectly from signals arising from the

interaction between the field and the external sensor. The related characterizations using phase-Doppler particle anemometer, laser Doppler velocimeter, particle image velocimetry, X-ray computerized tomography, electrical capacitance tomography, magnetic resonance imaging, to study multiphase flow, were all methods in which the external system provided the incident beams, be that light (Werther, 1999), laser (Zhou, Li, Chen, & Xu, 2000), X-ray (Wu, Cheng, Ding, Wei, & Jin, 2007; Wu, Cheng, Liu, & Jin, 2008), electrical field (Ceccio & George, 1996; Dyakowski, Jeanmeure, & Jaworski, 2000), magnetic field (Porion, Sommier, Faugere, & Evesque, 2004), to interact with the internal material in the field and generate informative signals (Powell, 2008). The corresponding flow field information can then be obtained via signal analysis.

Recently, positron emission tomography (PET) and positron emission particle tracking (PEPT) have been widely used to obtain detailed information on the motion and flow fields of fluids or granular materials in multiphase systems (Dewil, Baeyens, & Caerts, 2008; Hoffmann, Dechsiri, van de Wiel, & Dehling, 2005; Parker & Fan, 2008). These techniques are based on detecting the pairs of back-to-back γ -rays arising from annihilation of the emitted positrons. The positron-emitting tracers are normally labeled by the radionuclides ^{18}F , ^{61}Cu and ^{66}Ga . A positron camera and a location algorithm are used for calculating the tracer location and

* Corresponding author. Tel.: +86 10 62785464; fax: +86 10 62772051.

E-mail address: wf-dce@tsinghua.edu.cn (F. Wei).

Nomenclature

a	acceleration of particle (m/s^2)
A	section area of particle (m^2)
d	diameter of the particle (m)
D	diameter of the fluidized bed (m)
F	force (N)
g	acceleration of gravity (m/s^2)
m	mass of the particle (kg)
p	probability
Re	Renault number
s	signal A/D value
u	velocity of the particle (m/s)
C_D	draft force coefficient

Greek letters

ρ	density (kg/m^3)
μ	viscosity (Pa s)
σ	variance

Subscripts

b	buoyancy
g	gravity
m	mean
p	particle
D	draft force

speed. The labeled radioactive particles do not, however, memorize the data and the information recorded by the positron camera. Also reported was the computed tomographic scanner using γ -rays for the measurement of void fraction and its distribution in two-phase flow systems such as fluidized beds and bubble columns (Chaouki, Larachi, & Dudukovic, 1997; Kumar, Moslemian, & Dudukovic, 1995). Phosphorescent particles, too, can be used as tracers for experimental measurements of residence time distribution of solids for various kinds of reactors (Fan et al., 2002; Kim & Han, 2006; Wei, Wang, Jin, Yu, & Chen, 1994; Xu et al., 2004). If the tracer particles were “intelligent” enough to act as spies, capable of feeling and recording by themselves and sending information to the outside, we could know more of what happened in the reactor or the field.

To realize the particle spy concept, it is nowadays possible to encapsulate a sensor in a rigid enclosure to communicate externally, using available techniques of micro-electronics, micro-fabrication, micro-sensor, and computer technology (Jagtiani, Sawant, & Zhe, 2006; Song, Yuan, Tang, Song, & Ge, 2006). The mobile sensor, called Particle Measurement Sensor (PMS), can be appended to the measurement system to sense movement information, including acceleration, velocity, distance between particles, and so on. In addition, it can detect the field where it is located, including three-dimensional (3D) forces, temperature, pressure, and chemical components. The proposed method would not disturb the signal transfer in a light non-transparent system. The intelligent PMS is expected to be safe and cheap.

This article describes an example of PMS which utilized the 3D acceleration sensor to measure *in situ* particle movement information and the gravitational field to validate the particle-spy concept. The sensor was placed on a fluidized bed and the accelerations it felt were recorded, that is, the signals caused by collision with the emulsion/bubble phases and detected *in situ* by the PMS.

2. Experimental

2.1. Design of PMS

The PMS blueprint is an encapsulation of a micro 3D acceleration sensor, a microprocessor, together with a data communication interface into a small stainless steel ball in the form of a 60 mm-dia smart sphere, as illustrated in Fig. 1a. The micro-electro-mechanical system integrates sensors, actuators, electronics and mechanical features in a single microelectronic chip (MMA7260Q). The 3D acceleration sensor measures acceleration (change in speed) of anything that it's mounted on. It had a high sensitivity of 800 mV/g at 25 °C, with a noise level of less than 4.7 mV rms, and could measure a maximum acceleration of 6.0 g and a minimum acceleration of 0.04 g. This is a direct signal sensor comparable to a pressure detector or a capacitor detector. The analog signals derived as shown in Fig. 1a were converted into digital signals, by means of a Universal Serial Bus (USB) together with a RS232-to-USB interface (Fig. 1b). A battery was needed, as the circuit could operate only with an internal electricity source. An on-off switch was utilized to control the data processing and USB hold memory. All these were encapsulated

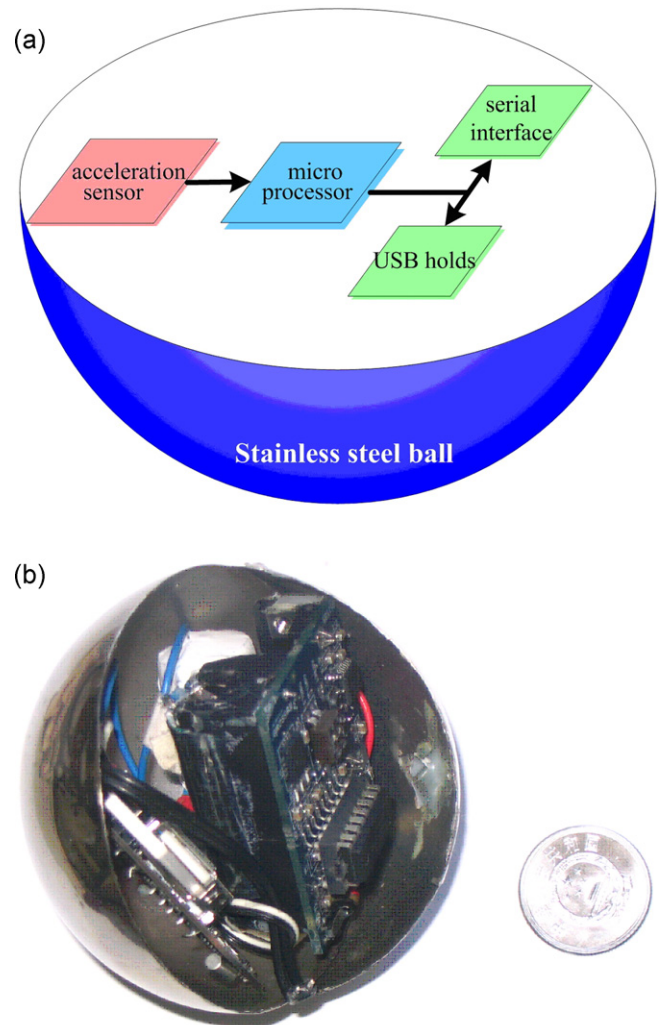


Fig. 1. (a) Design of prototype PMS: the 3D micro-acceleration sensor (MMA7260Q) feels movements and transfers the signals to the microprocessor (MC68HC908KX8), which processes the data and transfers them to the RS232 serial interface (MAX3316CAE). Information detected by PMS can be recorded by the USB holds *in situ*. The acceleration sensor, the microprocessor, the RS232 serial interface, and the USB holds are encapsulated in a 60 mm dia. stainless steel ball. (b) A PMS prototype.

into a stainless steel ball with a diameter of 60 mm, and a weight of 66 g, and the density of the PMS was 72 kg/m^3 . By adding other solid particles into the steel balls, or else by altering the thickness of the stainless steel ball, the density of the PMS can be further adjusted from 72 to 5000 kg/m^3 , though the encapsulation of the present PMS is far from fully optimized. The size of the PMS is large when dipped in a fluidized bed of fine powder. The interaction between the large PMS and fine fluidized particles is naturally very complex, calling for further study, while serving as a prototype in the present study.

2.2. Validation of PMS sensor by freefall

After encapsulation, a typical freefall experiment was performed on the PMS to identify which *in situ* measurement was easier. The PMS, fastened to a rope, was released to fall freely from a fixed height. With a flick of the on-off switch, 3D acceleration micro-sensor data were recorded in the USB hold. All digital signals perceived and transmitted by the sensor in free fall were collected by the USB hold at a sampling frequency of 100 Hz. After the freefall experiment, the USB holds were transferred from the PMS to a computer USB interface, and the data recorded by PMS were analyzed as shown in Section 3.2.

2.3. Phase structure detected by PMS

In this study, the PMS was employed as a spy to detect *in situ* particle fluidization behavior in a fluidized bed. The density of the PMS was first adjusted to 1200 kg/m^3 , and then the PMS was introduced into a 2800 mm-id by 260 mm-high air-fluidized bed (FB) consisting of $88.5\text{-}\mu\text{m}$ fluid catalytic cracking (FCC) catalyst particles with a density of 1710 kg/m^3 . The distance between the PMS, hung by a string at the center of the bed, and the FB distributor was about 300 mm. The signal collected by the PMS was sent out through the interface to a computer. With introducing air and increasing gas flow, the bed began to expand while bubble or emulsion phase interacted with the PMS, as signals of acceleration felt by the PMS during the collision process were recorded by the computer, through a wide range of gas velocities of 0.06–0.72 m/s, covering both the bubbling and turbulent regimes.

3. Results and discussion

3.1. Pristine signals of the acceleration sensor

The data recorded by the USB hold are digital values in the present prototype PMS. For a 3D acceleration micro-sensor, the data consisted of a four-dimensional array of time, and X, Y, and Z sensor directions. The acceleration recorded by the PMS was always 1.0 g for the present operation in the gravitational field. The components X, Y, and Z sensor directions could be changed with the orientation of the PMS, though the synthetic acceleration was always 1.0 g. For us, the PMS sensor was stationary, and the acceleration observed should be 0 g. Thus, the data recorded by PMS sensor should be compensated for the gravitational field (1.0 g).

For freefall, the PMS orientation was tailored to make freefall in the Z direction, to thus facilitate data analysis and understanding what happened to the PMS. The freefall PMS signals shown in Fig. 2, display sudden changes in digital acceleration values at the start of the PMS descent for all the X, Y, and Z directions: 75–139 cps for the Z sensor direction while the values for X or Y sensor remained almost unchanged. The freefall experiment beginning with PMS release from the rope is shown to be not easy to achieve. Little rotation of the PMS was detected (i.e., the peak signal at the beginning of freefall, as shown in Fig. 2).

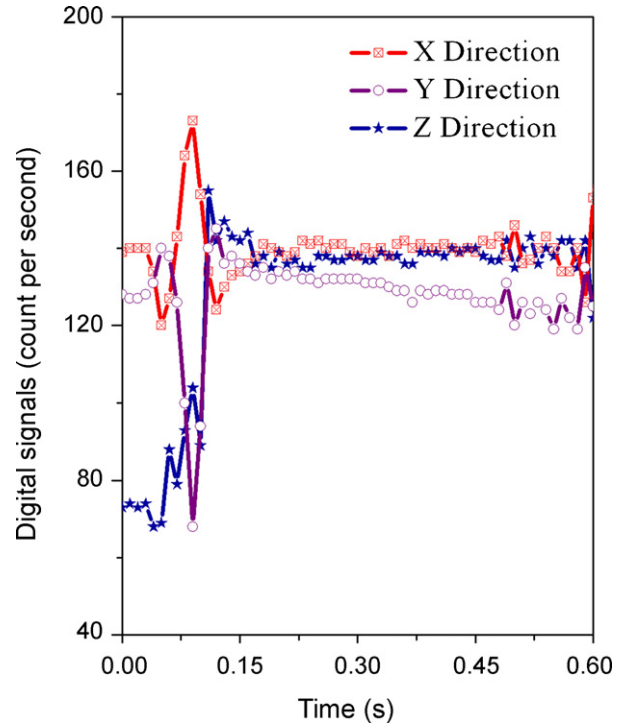


Fig. 2. Digital signals of PMS during free fall in a fluidized bed of FCC catalyst particles.

3.2. Validation of PMS sensor by freefall

3.2.1. Acceleration of the PMS and the gravitational field information

According to the sensor specification, the PMS acceleration was in direct proportion to the A/D value and could be formulated as

$$a_{\text{ins}} = \frac{S_{\text{ins}} - S_{\text{bas}}}{64}, \quad (1)$$

where S_{ins} is the A/D value at a given instant, and S_{bas} is the baseline for the static PMS. The acceleration calculated from Eq. (1) during freefall is illustrated in Fig. 3, showing that the values for the X and Y directions during freefall were almost 0, while that for the Z direction was nearly 1.0 g (with gravitational field compensation), that is, there were practically no forces in the X and Y directions and freefall occurred only in the Z direction due to gravitational field. At the start of freefall, the X, Y, and Z direction values were 0.2-g, 0.2-g, and 1.1-g, respectively, implying relatively weak forces in the X and Y directions as compared to the Z direction. This was possibly caused by rotation of PMS at the beginning of the freefall. However, this duration was very short and the effect was small, thus we shall disregard rotation in the following discussion.

3.2.2. Instantaneous velocity and displacement of PMS

The PMS was subjected to three kinds of forces during freefall (McCabe, Smith, & Harriott, 1992). The first is gravity, which is equal to mg ; where, m is the mass of PMS, and g is the acceleration of gravity. The second is buoyancy, which is expressed in the following equation:

$$F_b = -\frac{1}{6}\pi d_p^3 \rho g. \quad (2)$$

The last is drag force, which can be described as

$$F_D = -C_D A_p \frac{\rho u^2}{2}. \quad (3)$$

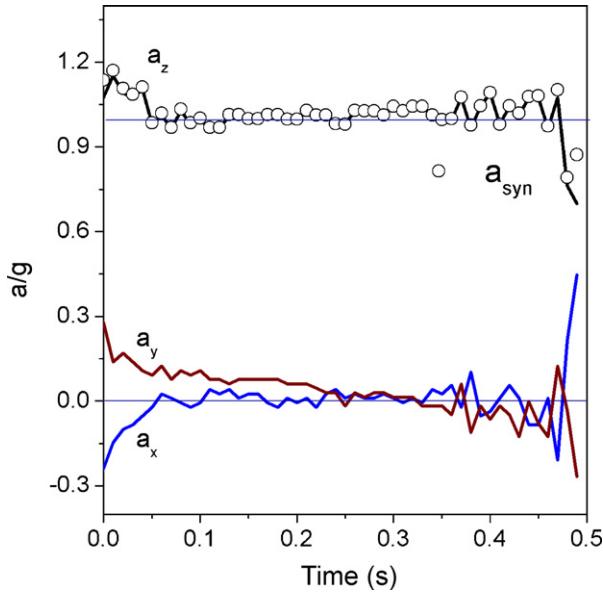


Fig. 3. PMS acceleration during the freefall process ($g=9.81 \text{ m/s}^2$).

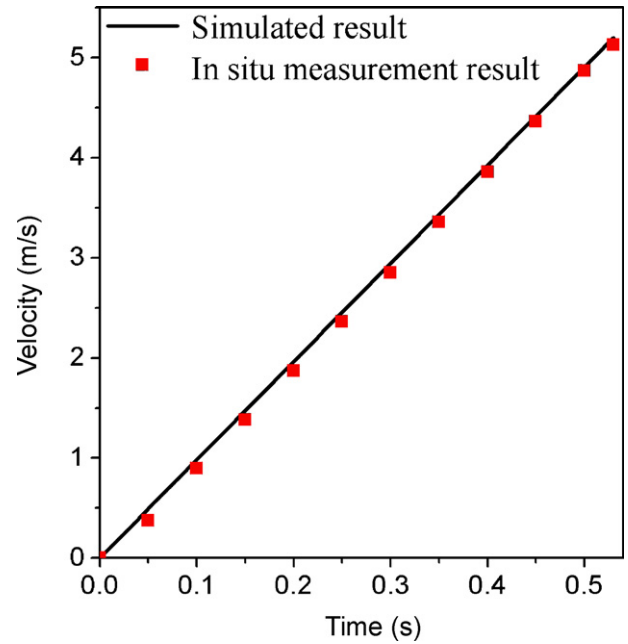


Fig. 4. PMS velocity during the freefall process.

While the PMS sensor moves in the laminar flow state ($Re_p = (\rho_p u d / \mu) < 2$), C_D is expressed as

$$C_D = \frac{24}{Re_p} \quad (4)$$

When velocity increases, the PMS sensor is in a transition state, wherein $2 < Re_p < 1000$, then C_D is given by

$$C_D = \frac{18.5}{Re_p^{0.6}} \quad (5)$$

During freefall, the net resultant force on the PMS sensor is

$$F = F_g - F_b - F_D = mg - \frac{1}{6} \pi d_p^3 \rho g - C_D A_p \frac{\rho u^2}{2} \quad (6)$$

While falling, the MPS particle velocity increased, and its movement entered the transition state, thus allowing us to use Eqs. (4) and (5) to compute F , without considering the turbulent flow state. The simulated results by the above model are illustrated in Fig. 4 for velocity and in Fig. 5 for displacement, calculated by numerical integration based on the data from the PMS:

$$v_i = v_{i-1} + \frac{a_{i-1} + a_i}{2} \Delta t, \quad (7)$$

$$s_i = s_{i-1} + \frac{v_{i-1} + v_i}{2} \Delta t. \quad (8)$$

Eq. (7) was used to calculate the instantaneous velocity of the PMS sensor shown in Fig. 4, which is consistent with the ideal freefall model. The PMS records can track itself and provide us with the *in situ* measurement result. The greatest error was about 3% at the beginning of freefall possibly due to the non-ideal freefall process of the experiment, but it is trivial. Eq. (8) was used to calculate the instantaneous displacement of the particle shown in Fig. 5. Such computation confirmed the freefall model. At the end of the freefall, the PMS had fallen 1.34 m by integration of acceleration recorded by the PMS, which checks the result calculated from the ideal freefall model, 1.36 m, with an error of about 1.5%.

The validation experiment indicated that the PMS is a sensitive sensor capable of recording the trajectory of itself. Here it should be mentioned that the sampling frequency was 100 Hz and the minimum acceleration which could be recorded was 0.04-g. However, some instantaneous information, such as high frequency collisions

in a real fluidized bed or trivial interaction with fine fluidized particles, could not be recorded faithfully by the present PMS system. Also the algorithm needs revision if the rotation of PMS is considered. Detailed study for complex trajectory is still needed in future work. The next section will show how flow regime maps can be obtained from the time series of acceleration measurements.

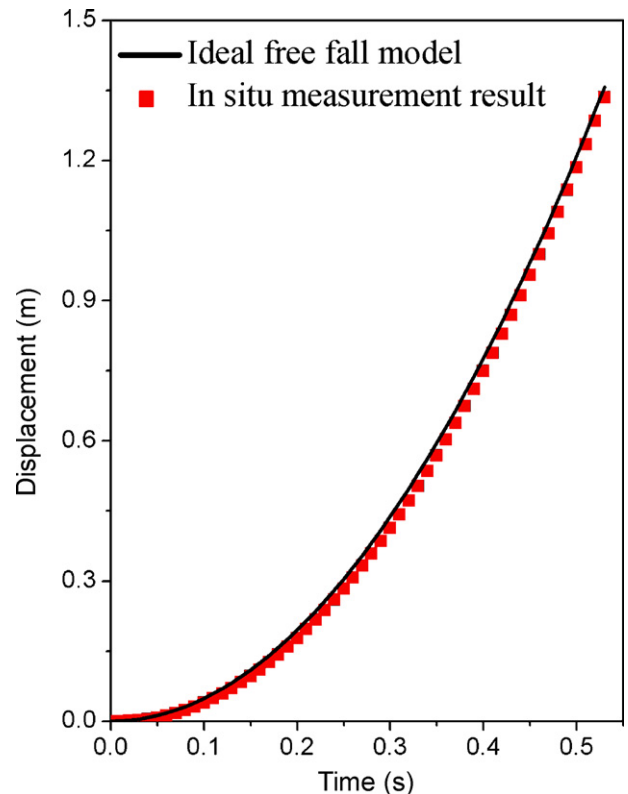


Fig. 5. PMS displacement during the freefall process.

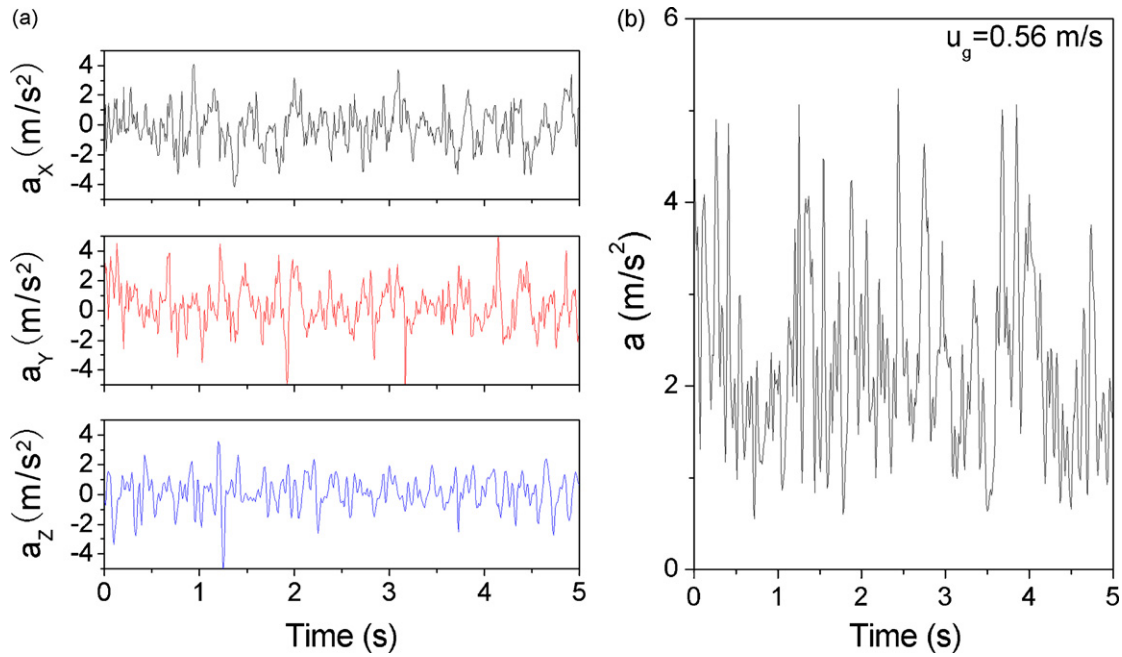


Fig. 6. Signal time series of PMS as detector in fluidized bed of FCC catalyst with apparent gas velocity of 0.56 m/s, where (a) refers to signals of three acceleration components and (b) represents synthetic acceleration.

3.3. Phase structure of fluidized bed as indicated by PMS

3.3.1. The time series of the acceleration

Fig. 6a illustrates typical acceleration signals obtained by PMS in the fluidized bed for the three directions X, Y and Z, which could be combined into the following synthetic acceleration by removing the

information on direction yet preserving the value of acceleration, as shown in Fig. 6b:

$$a = \sqrt{a_x^2 + a_y^2 + a_z^2} \tag{9}$$

An acceleration peak is shown in the signal time series when a bubble hits the PMS, while the signals at the baseline are mainly contributions from collisions between the emulsion phase and the PMS. Then the interaction can be recorded as a 3D vector. Collision direction is however not well understood because of the complexity of movement between PMS and bubbles in the fluidized bed.

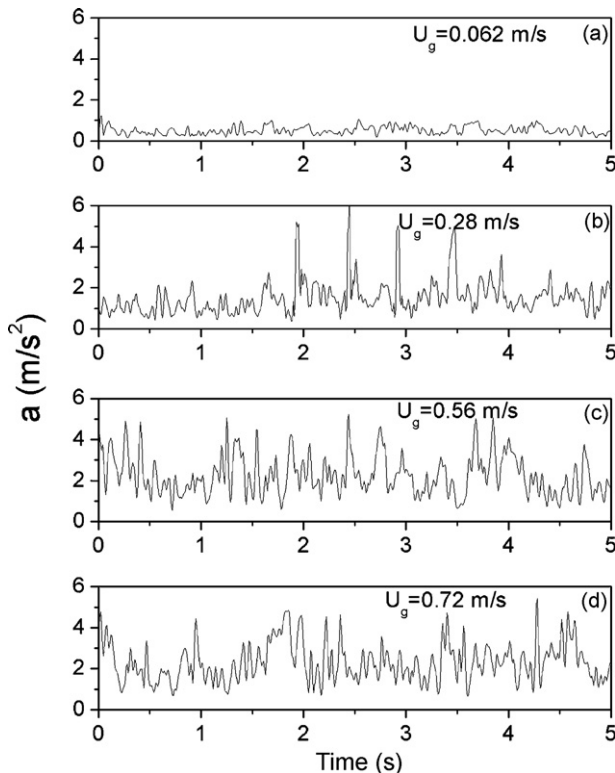


Fig. 7. Synthetic acceleration signal time series of PMS as detected in FCC catalyst fluidized bed, for various apparent gas velocities.

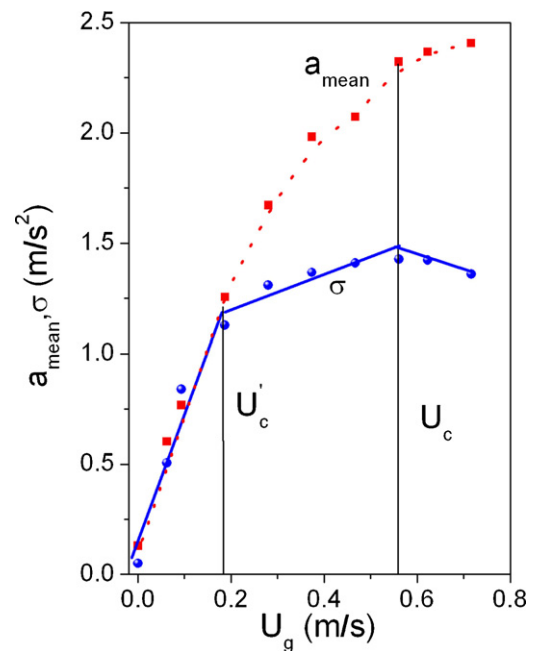


Fig. 8. Average and variance of synthetic acceleration signal time series of PMS as detected in a FCC catalyst fluidized bed for various apparent gas velocities.

The following discussion involving the synthetic acceleration will facilitate further analysis of the signals from PMS.

Fig. 7 displays the time series of synthetic accelerations with various superficial gas velocities. At the gas velocity of 0.062 m/s, the FCC catalyst starts to exhibit bubbling fluidization; yielding stable time series of acceleration of approximately 0.8 m/s² with small variance, and with only a small peak at 3.2 s with a height of 3.5 m/s² while a bubble hits the sensor. Peaks were scarce, marking homogeneous fluidization with low bubble holdup while the particles were in a stable fluidization state, and the pressure drop changed with minor fluctuations. When the gas velocity increased to 0.28 m/s, fluctuation in acceleration increased perceptibly as illustrated in Fig. 7b. A strong peak with an intensity of approximately 5.0 m/s² is displayed, followed by even stronger peaks as the powder behaved in the bubbling fluidization state. When the gas velocity was raised to 0.56 m/s, fluidization reached the turbulent state, as the baseline became higher and bed fluctuation became more obvious. When the gas velocity increased to 0.72 m/s, the intensity of acceleration increased even more perceptibly.

As shown in Fig. 8, the average acceleration increases with gas velocity, indicating increasing force between the PMS and the particles or bubbles in the fluidized bed. When the gas velocity is less

than 0.19 m/s, the variance increases rapidly with gas velocity. With gas velocity in the range between 0.19 and 0.56 m/s, the variance increases but slowly, to reach a maximum value of 1.43 m/s², after which the variance begins to decrease. Variance denotes the fluctuation of PMS acceleration in the fluidized bed, which is related to the phase structure. The results obtained by PMS exhibit similar trends as by pressure drop; both with maxima in variance. As with other characterization methods, the transition point from bubbling to turbulent fluidization can be easily obtained by variance analysis. For FCC catalyst systems, the following equation formulated by Cai, Jin, and Yu (1991) by correlating experimental results of various Groups A, B particles, was utilized to compute U_c :

$$\frac{U_c}{\sqrt{gd_p}} = \left(\frac{\mu_{f0}}{\mu_f} \right)^{0.2} \left[K \left(\frac{\rho_{f0}}{\rho_f} \right) \left(\frac{\rho_p - \rho_f}{\rho_f} \right) \left(\frac{D}{d_p} \right) \right]^{0.27}, \quad (10)$$

where

$$K = \left(\frac{0.211}{D^{0.27}} + \frac{2.42 \times 10^{-3}}{D^{1.27}} \right)^{1/0.27}. \quad (11)$$

The result was $U_c = 0.57$ m/s, which checks our experimental finding of the maximum variance at 0.56 m/s.

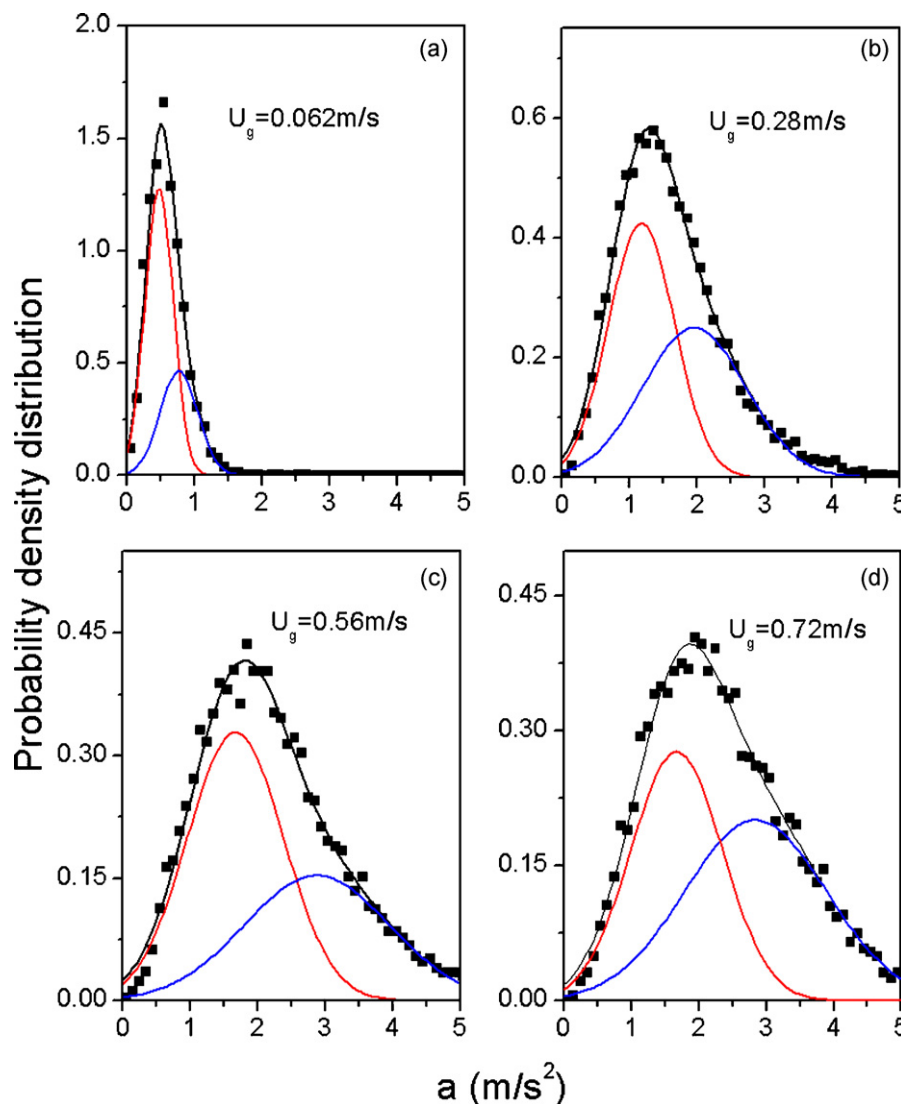


Fig. 9. Probability density distribution (PDD) of synthetic acceleration signals with various apparent gas velocities for FCC catalysts fluidized bed.

3.3.2. Probability density distribution of acceleration

The acceleration signals of PMS consist of a series of acceleration caused by the collisions between PMS and the emulsion (cluster or dense)/bubble (void or dilute) phase in the fluidized bed. These were converted by Fourier transformation into probability density distribution, as illustrated in Fig. 9.

The probability density distribution (PDD) of the acceleration time series can be considered as the combination of two Gaussian distributions with different means and variances of the bubble and emulsion, having small density and high velocity for the former, and otherwise for the latter with stronger momentum interchange. As shown in Fig. 9, the peak with higher acceleration is attributed to the bubble (void or dilute) phase, while the other, to the emulsion (cluster or dense) phase. Thus, the PDD can be divided into two peaks.

The PDD curves of the acceleration time series with different gas velocities shown in Fig. 9 can be divided into the contributions from the bubble and from the emulsion phases, as follows:

$$p(a) = \frac{1 - \phi}{\sqrt{2\pi}\sigma_m} e^{-((a-a_m)^2/2\sigma_m^2)} + \frac{\phi}{\sqrt{2\pi}\sigma_b} e^{-((a-a_b)^2/2\sigma_b^2)}. \quad (12)$$

Accelerations and variance are plotted against apparent gas velocity in Fig. 10 to show how both increase with gas velocity for both the bubble phase and the emulsion phase. Different from acceleration, variance, which reflects the degree of fluctuation of the force between the PMS and the emulsion/bubble phase, first increases to a maximum at the gas velocity of 0.56 m/s, and then gradually decreases. This indicates that both the bubble and the emulsion phases exhibit stronger fluctuation at the transition from bubbling fluidization to turbulent fluidization (Andreux, Gauthier, Chaouki, & Simonin, 2005; Lin, Wei, & Jin, 2001). After reaching the turbulent state, force fluctuation for FCC particles remains essentially constant. To reflect the difference in fluctuation between the bubble and emulsion phases with PMS, the following ratio of their fluctuations, σ_{be} , is proposed:

$$\sigma_{be} = \frac{\sigma_b - \sigma_e}{\sigma_e - \sigma_0}, \quad (13)$$

where σ_b , σ_e , and, σ_0 refer to the variance of bubble phase, emulsion phase, and background of the PMS sensor, respectively. Fig. 10

shows that the maximum of σ_{be} was detected at the point when U_c' was 0.19 m/s, indicating that the difference of acceleration fluctuation between the bubble and emulsion phase interacting with PMS reached a maximum as reported by Andreux et al. (2005). Below U_c' , the fluidized bed consists predominantly of aerated emulsion, while with increasing fluidizing velocity, bubbling takes over (Andreux et al., 2005). According to Andreux et al. (2005), when the fluidizing velocity reaches U_c' , aeration from the bubble phase begins to predominate, though increasing the fluidizing velocity above U_c' does not much change bed aeration, until when the fluidizing velocity reaches U_c at which σ_{be} begins to increase. That is, a phase structure transformation occurs at U_c' and at U_c , as confirmed in Figs. 8 and 10.

Based on details captured from the statistical and PDD analyses of the time series of acceleration, the phase structure can be determined. It is commonly believed that when superficial gas velocity increases, bubbling fluidization, turbulent fluidization, and fast fluidization will be detected in the above order (Andreux et al., 2005; Bai, Issangya, & Grace, 1999; Bai, Shibuya, Nakagawa, & Kato, 1996; Liang et al., 1997; Makkawi & Wright, 2002; Mostoufi & Chaouki, 2004; Yang, Du, & Fan, 2007; Zhu, Zhu, Li, & Li, 2008). In the said flow patterns, there exist both the bubble (void or dilute) phase and emulsion (cluster or dense) phase in the fluidized bed. In the bubbling fluidization state, the void phase was dispersed while the cluster phase was continuous. In the fast fluidization state, the cluster phase was dispersed while the void phase was continuous. Turbulent fluidization is a transition state, in which there is no visible continuous phase (Bai et al., 1996; Liang et al., 1997; Lin et al., 2001; Makkawi & Wright, 2002; Mostoufi & Chaouki, 2004). In our study, bubbling fluidization and turbulent fluidization were shown. As illustrated in Figs. 8 and 10, there was a transition before U_c , that is, U_c' at 0.19 m/s, confirming the new description of fluidization regimes proposed by Andreux et al. based on recent data on pressure fluctuation, ratio of bubble velocity to emulsion velocity, and bubble frequency (Andreux et al., 2005). Before the U_c' , the PMS collided mainly with particles, while the bubble phase contributed not significantly, as indicated in Fig. 8. When gas velocity increased, the bubble phase increased, and likewise the variance of acceleration.

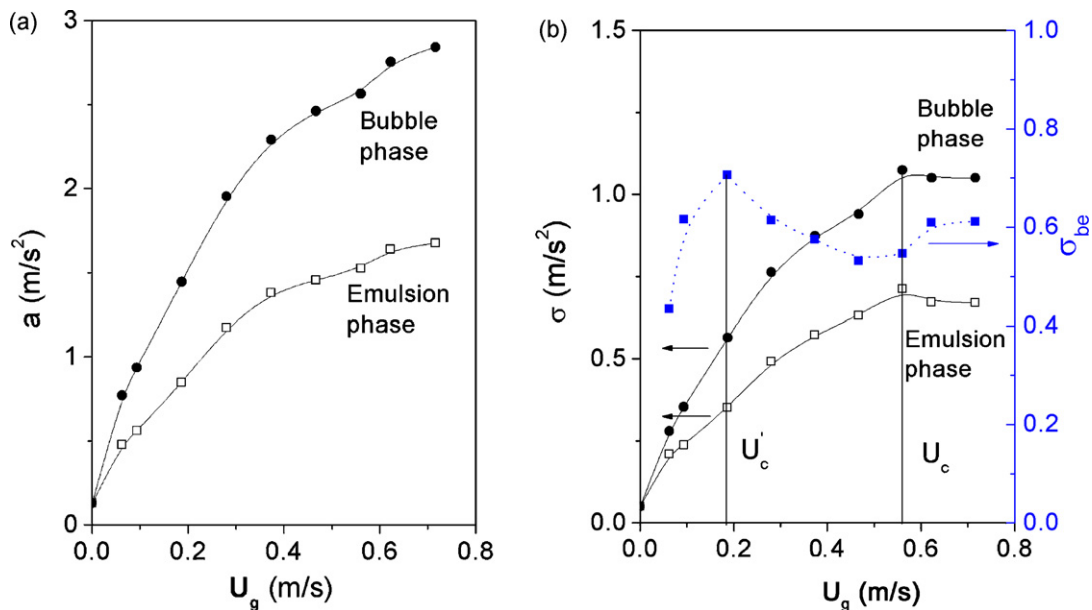


Fig. 10. Acceleration (a) and variances (b) of bubble and emulsion phases for PDD for FCC catalyst.

Finally, it should be noted that our PMS with a 3D acceleration micro-sensor was merely a model PMS used to demonstrate the concept of the particle spy. The freefall experiment proved that PMS recorded both *in situ* measurements, such as field information, acceleration, velocity, and displacement. For a well-sealed PMS, which can separate the liquid (such as water and ethanol) from the PCB layer, it can work in liquid–solid systems, detecting *in situ* interaction between the PMS and bubbles, for liquid chemical reactors (Yang et al., 2007) such as in the mining industry (Nguyen, Nalaskowski, & Miller, 2003; Preuss & Butt, 1999), instead of external sensors (Nespolo, Chan, Grieser, Hartley, & Stevens, 2003; Vakarelski et al., 2008), to provide a new viewpoint for those studies. For high temperature and corrosive and toxic liquids, PMS needs adequate encapsulation especially to protect the electronics from temperatures exceeding 400 °C. The PMS can be integrated with other sensors, including thermocouples, gyroscopes, and pressure gauges, to enhance its functionality.

4. Conclusions

In this research, the concept of a particle spy was tested in the form of an encapsulated prototype Particle Measurement Sensor (PMS), 60 mm in diameter, including communication parts and USB holds. The freefall movement of PMS was utilized to validate the proposed measurement technology. The acceleration, instantaneous velocity, and instantaneous displacement were obtained by *in situ* measurement. While hanging the PMS in a fluidized bed of FCC particles, the PMS records *in situ* the acceleration time series, to reveal the phase structure (bubble and emulsion) transition in the fluidized bed. The transition point at which the two phases begin to coalesce can be obtained from the difference between the variances of the bubble and of the emulsion phases. The transition point where the two phases separate represents the shift from bubbling fluidization to turbulent fluidization, and is indicated by the maximum acceleration variance, where the fluctuation is strongest. This information is crucial to understanding the phase structure in the fluidized bed. Although the complex trajectory cannot be obtained in the present study, and the size of PMS is large, the prototype for an intelligent particle was shown. The performance of the present prototype PMS is expected to improve should the size of PMS be decreased to, say, several to tens micrometers with delicate encapsulation of the sensors. The more the sensors encapsulated, the more additional information obtained by *in situ* measurement.

Acknowledgment

The work was supported by the Foundation for Natural Scientific Foundation of China (No. 20606020, No. 20736004, No. 20736007).

References

- Andreu, R., Gauthier, T., Chaouki, J., & Simonin, O. (2005). New description of fluidization regimes. *AIChE Journal*, 51(4), 1125–1130.
- Bai, D., Issangya, A. S., & Grace, J. R. (1999). Characteristics of gas–fluidized beds in different flow regimes. *Industrial & Engineering Chemistry Research*, 38(3), 803–811.
- Bai, D., Shibuya, E., Nakagawa, N., & Kato, K. (1996). Characterization of gas fluidization regimes using pressure fluctuations. *Powder Technology*, 87(2), 105–111.
- Bi, H. T., & Grace, J. R. (1995). Flow regime diagrams for gas–solid fluidization and upward transport. *International Journal of Multiphase Flow*, 21(6), 1229–1236.
- Cai, P., Jin, Y., & Yu, Z. Q. (1991). Effect of operation temperature on transition from bubbling to turbulent fluidization. *Chemical Engineering*, 19(3), 62–66 (in Chinese).
- Ceccio, S. L., & George, D. L. (1996). A review of electrical impedance techniques for the measurement of multiphase flows. *Journal of Fluids Engineering-Transactions of the ASME*, 118(2), 391–399.
- Chaouki, J., Larachi, F., & Dudukovic, M. P. (1997). Noninvasive tomographic and velocimetric monitoring of multiphase flows. *Industrial & Engineering Chemistry Research*, 36(11), 4476–4503.
- Cheng, Y., Wu, C. N., Zhu, J. X., Wei, F., & Jin, Y. (2008). Downer reactor: From fundamental study to industrial application. *Powder Technology*, 183(3), 364–384.
- Dewil, R., Baeyens, J., & Caerts, B. (2008). CFB cyclones at high temperature: Operational results and design assessment. *Particuology*, 6(3), 149–156.
- Dyakowski, T., Jeanmeure, L. F. C., & Jaworski, A. J. (2000). Applications of electrical tomography for gas–solids and liquid–solids flows—A review. *Powder Technology*, 122(3), 174–192.
- Fan, Y. P., Ye, S., Chao, Z. X., Lu, C. X., Sun, G. G., & Shi, M. X. (2002). Gas–solid two-phase flow in FCC riser. *AIChE Journal*, 48(9), 1869–1887.
- Hoffmann, A. C., Dechshiri, C., van de Wiel, F., & Dehling, H. G. (2005). PET investigation of a fluidized particle: Spatial and temporal resolution and short term motion. *Measurement Science & Technology*, 16(3), 851–858.
- Jagtiani, A. V., Sawant, R., & Zhe, J. (2006). A label-free high throughput resistive-pulse sensor for simultaneous differentiation and measurement of multiple particle-laden analytes. *Journal of Micromechanics and Microengineering*, 16(8), 1530–1539.
- Kim, J., & Han, G. Y. (2006). Effect of agitation on fluidization characteristics of fine particles in a fluidized bed. *Powder Technology*, 166(3), 113–122.
- Kumar, S. B., Moslemian, D., & Dudukovic, M. P. (1995). A gamma-ray tomographic scanner for imaging voidage distribution in 2-phase flow systems. *Flow Measurement and Instrumentation*, 6(1), 61–73.
- Kwauk, M., Li, J. H., & Liu, D. J. (2000). Particulate and aggregative fluidization—50 years in retrospect. *Powder Technology*, 111(1/2), 3–18.
- Liang, W. G., Zhang, S. L., Zhu, J. X., Jin, Y., Yu, Z. Q., & Wang, Z. W. (1997). Flow characteristics of the liquid–solid circulating fluidized bed. *Powder Technology*, 90(2), 95–102.
- Lin, Q., Wei, F., & Jin, Y. (2001). Transient density signal analysis and two-phase micro-structure flow in gas–solids fluidization. *Chemical Engineering Science*, 56(6), 2179–2189.
- Makkawi, Y. T., & Wright, P. C. (2002). Fluidization regimes in a conventional fluidized bed characterized by means of electrical capacitance tomography. *Chemical Engineering Science*, 57(13), 2411–2437.
- McCabe, W. L., Smith, J. C., & Harriott, P. (1992). *Unit operation in chemical engineering*. New York: McGraw-Hill.
- Mostoufi, N., & Chaouki, J. (2004). Flow structure of the solids in gas–solid fluidized beds. *Chemical Engineering Science*, 59(20), 4217–4227.
- Nespolo, S. A., Chan, D. Y. C., Grieser, F., Hartley, P. G., & Stevens, G. W. (2003). Forces between a rigid probe particle and a liquid interface: Comparison between experiment and theory. *Langmuir*, 19(6), 2124–2133.
- Nguyen, A. V., Nalaskowski, J., & Miller, J. D. (2003). A study of bubble–particle interaction using atomic force microscopy. *Minerals Engineering*, 16(11), 1173–1181.
- Parker, D. J., & Fan, X. F. (2008). Positron emission particle tracking—Application and labelling techniques. *Particuology*, 6(1), 16–23.
- Porion, P., Sommier, N., Faugere, A. M., & Evesque, P. (2004). Dynamics of size segregation and mixing of granular materials in a 3D-blender by NMR imaging investigation. *Powder Technology*, 141(1/2), 55–68.
- Powell, R. L. (2008). Experimental techniques for multiphase flows. *Physics of Fluids*, 20(4) (Art. No. 040605).
- Preuss, M., & Butt, H. J. (1999). Direct measurement of forces between particles and bubbles. *International Journal of Mineral Processing*, 56(1–4), 99–115.
- Song, G. M., Yuan, H. Y., Tang, Y., Song, Q. J., & Ge, Y. J. (2006). A novel three-axis force sensor for advanced training of shot-put athletes. *Sensors and Actuators A-Physical*, 128(1), 60–65.
- Vakarelski, I. U., Lee, J., Dagastine, R. R., Chan, D. Y. C., Stevens, G. W., & Grieser, F. (2008). Bubble colloidal AFM probes formed from ultrasonically generated bubbles. *Langmuir*, 24(3), 603–605.
- Wei, F., Wang, Z. W., Jin, Y., Yu, Z. Q., & Chen, W. (1994). Dispersion of lateral and axial solids in a cocurrent downflow circulating fluidized-bed. *Powder Technology*, 81(1), 25–30.
- Wei, F., Zhang, Q., Qian, W. Z., Yu, H., Wang, Y., Luo, G. H., et al. (2008). The mass production of carbon nanotubes using a nano-agglomerate fluidized bed reactor: A multiscale space-time analysis. *Powder Technology*, 183(1), 10–20.
- Werther, J. (1999). Measurement techniques in fluidized beds. *Powder Technology*, 102(1), 15–36.
- Wu, C. N., Cheng, Y., Ding, Y. L., Wei, F., & Jin, Y. (2007). A novel X-ray computed tomography method for fast measurement of multiphase flow. *Chemical Engineering Science*, 62(16), 4325–4335.
- Wu, C. N., Cheng, Y., Liu, M. L., & Jin, Y. (2008). Measurement of axisymmetric two-phase flows by an improved x-ray-computed tomography technique. *Industrial & Engineering Chemistry Research*, 47(6), 2063–2074.
- Xu, J. A., Bao, X. J., Wei, W. S., Shi, G., Shen, S. K., Bi, H. T., et al. (2004). Statistical and frequency analysis of pressure fluctuations in spouted beds. *Powder Technology*, 140(1/2), 141–154.
- Yang, G. Q., Du, B., & Fan, L. S. (2007). Bubble formation and dynamics in gas–liquid–solid fluidization—A review. *Chemical Engineering Science*, 62(1/2), 2–27.
- Zhou, L. X., Li, Y., Chen, T., & Xu, Y. (2000). Studies on the effect of swirl numbers on strongly swirling turbulent gas–particle flows using a phase-Doppler particle anemometer. *Powder Technology*, 112(1/2), 79–86.
- Zhu, H. Y., Zhu, J., Li, G. Z., & Li, F. Y. (2008). Detailed measurements of flow structure inside a dense gas–solids fluidized bed. *Powder Technology*, 180(3), 339–349.
- Zhu, J. X., Yu, Z. Q., Jin, Y., Grace, J. R., & Issangya, A. (1995). Cocurrent downflow circulating fluidized-bed (downer) reactors—A state-of-the-art review. *Canadian Journal of Chemical Engineering*, 73(5), 662–677.